Surface magnetism at the Néel temperature of an $FeBO_3$ single crystal

B. Stahl,[1,*] S. Bhattacharya,[1] S. Gottschalk,[1] J. Ellrich,[1] H. Schmitt,[1] J. Ebert,[1] M. Ghafari,[1] H. Hahn,[1] A. Kamzin,[2] D. Vcherashniy,[2] and A. R. Raju[3]

[1]*Fachbereich Material- und Geowissenschaften, Petersenstrasse 23, TU Darmstadt, 64287 Darmstadt, Germany*

[2]*Laboratory of Magnetism, A.F. Ioffe Physical-Technical Institute, Politekhnicheskaya 26, St. Petersburg, 194021, Russia*

[3]*Chemistry and Physics of Materials Unit, Jawaharlal Nehru Centre for Advanced Scientific Research, Jakkur, Bangalore 560 064, India*

(Received 3 June 2002; published 27 September 2002)

In the near-surface region of an $FeBO_3$ single crystal a new magnetic-phase transition was discovered at the bulk Néel point by depth selective Mössbauer spectroscopy. The results neither fit into the concept of an ordinary nor that of an extraordinary type of surface transition. The sublattice magnetization dynamics of the near-surface phase is changed with respect to that of the bulk and exhibits similarities to that of a superparamagnetic system. In the same way as the Mössbauer line shape reveals the critical slowing down in the time-correlation function of the local moment, the increase in thickness of the near-surface region mirrors the divergence of the correlation length in the system when approaching the Néel temperature. The results on the pure $FeBO_3$ crystal are compared to those gained by replacing one-quarter of the Fe atoms by Ga. The phase transition in the $FeBO_3$ single crystal was studied from 291 K up to the Néel temperature $T_N = 348.35$ K by depth selective conversion electron Mössbauer spectroscopy in an ultrahigh vacuum of 10^{-9} mbar.

DOI: 10.1103/PhysRevB.66.104426 PACS number(s): 75.70.Rf, 68.08.Bc, 87.64.Pj, 68.18.Jk

I. NEAR-SURFACE MAGNETISM AT PHASE TRANSITIONS

One of the first phenomenological treatments of the impact of the surface on the magnetic ordering of the nearest atomic layers was given by Néel.[1] Developments on this theory can be found in the work by Bogdanov *et al.*[2,3] With the aid of computer simulations the insight into the scenario of near-surface magnetism could be improved and critical laws and exponents of various quantities could be established.[4–8] In general the surface exchange coupling need not be the same compared to the bulk material. In the case of an enhanced surface coupling the magnetic ordering is expected to show up above the bulk transition temperature in a near-surface region that is given by the magnetic correlation length. Below the bulk transition temperature the surface should exhibit an enhanced order-parameter value. In the case of a diminished surface coupling the whole semi-infinite sample should show magnetic ordering only below the bulk transition temperature. Nevertheless, the order-parameter value of the surface will be lowered at any temperature compared to the bulk value. A transition region between surface and bulk will again be defined by the magnetic correlation length.[9]

Near-surface magnetism, in relation to critical phenomena, was first studied on ultrafine particles[10,11] and then extended to thin films.[12] In small particles the idea is to attribute the size dependence of the measured parameters to the surface. In thin films or semi-infinite systems, the experimental methods have to fulfill the demanding requirements with respect to phase characterization and depth resolution. Scattering techniques with polarized particles in ultrahigh vacuum usually probe the topmost atomic layers without giving information on the subsequent regions in the sample. As they measure the change in polarization of the scattered particles, their application is restricted to ferromagnets. Watson *et al.*[13] developed evanescent magnetic x-ray scattering to get the information on a near-surface region of semi-infinite systems. The recent improvements in nuclear resonant scattering of synchrotron radiation provide a similar depth resolution and include information on the magnetic ordering via the hyperfine interaction.[15,16] It has yet to be applied to this field. The pioneering work on the temperature dependence of the order parameter near the surface of an antiferromagnet was carried out on ultrafine hematite particles by van der Kraan[17] and Shinjo *et al.*[18] decades ago. The results revealed a magnetic behavior of the first few atomic layers on the surface of the crystallites that was different in comparison to that of the bulk. The first DCEMS (Depth Selective Conversion Electron Mössbauer Spectroscopy) experiment on a polycrystalline hematite film at room temperature,[19] gave a thickness of 1.8 nm to the magnetically distinct near-surface region. These results could be confirmed by our own DCEMS measurements for the surface of a hematite single crystal.[20] The same crystal was also used to study the near-surface behavior at the spin reorientation transition, the so-called Morin transition at 260 K.[21]

The extreme difficulty of characterizing the magnetic state close to a phase transition as a function of temperature and depth under ultrahigh vacuum is responsible for a lack of hard experimental tests of the theoretical background. Depth selective Mössbauer spectroscopy[22,23] as a nondestructive method in ultrahigh vacuum satisfies both requirements: Mössbauer spectroscopy gives quantitative results on the average value of the order parameter of a magnetic system as well as its dynamical features. It can be easily applied to antiferromagnets, avoiding stray field contributions to the Hamiltonian that occur in ferromagnets. Also the ability of depth selection allows us to study the interesting magnetic quantities as a function of depth. Such a depth selective experimental study is vital for testing the full implications of the theories on surface critical phenomena. To our knowl-

edge, only evanescent magnetic x-ray scattering on a single crystal of UO_2 at a synchrotron radiation facility was able to fulfill part of these requirements.[13] Nevertheless, it was not possible to determine the depth dependence of the magnetic ordering with sufficient precision, as the depth weight functions involved are pure exponentials. In addition, x-ray scattering cannot characterize the magnetic order parameter in as direct and as unambiguous a manner as in Mössbauer spectroscopy.

II. DCEMS ON A $FeBO_3$ SINGLE CRYSTAL

As a consequence of the adequate features of the DCEMS method, experiments to study near-surface magnetism close to a critical point could be performed on single crystals. Single crystals constitute the simplest and cleanest system where the pure influence of the surface on the magnetic ordering can be studied. In experiments on ultrafine particles and thin films not only can the presence of a surface or interface change the magnetic behavior, but uncontrollable structural inhomogeneities can also play an important role. For instance, it is well known that otherwise unstable crystallographic phases are stabilized in small particles at room temperature. In the case of thin films the epitaxial interplay between substrate and film has to be taken into account.

With the DCEMS technique a near-surface region of 1 to 300 nm in depth could be probed with sufficient statistical quality. As hematite with its high Néel temperature of 956 K is not a feasible candidate to study the antiferromagnetic to paramagnetic phase transition, an $FeBO_3$ crystal was chosen for this purpose.[14] $FeBO_3$ has a rather similar crystal and magnetic structure compared to hematite. Its Néel temperature of 348.35 K makes it an ideal sample for the present characterization. Due to the elevated temperature the surface of the crystal could be held clean of adsorbates during the duration of the experiment. The time period amounted to several weeks of measurement. To ensure the highest possible experimental sensitivity, the single crystal was fully enriched in the Mössbauer isotope ^{57}Fe. The $FeBO_3$ single crystal was synthesized by the flux method. Its surface was subsequently thinned down by mechanical and chemical polishing. Thus a structurally homogenous sample was obtained. The *c* axis of the single crystal was perpendicular to the studied surface. The magnetic moments in this antiferromagnet, with a weak parasitic moment due to spin canting, lie in plane. The smoothness of the surface was checked by atomic force microscopy (AFM). On areas of $5\ \mu m \times 5\ \mu m$, which are macroscopic compared to the probing thickness of the DCEMS experiments, only rare steps of the size of a single lattice constant were found. As a consequence, the determined roughness of 0.4 nm is more a sign of the noise of the AFM than the real geometrical roughness of the sample.

First depth selective Mössbauer investigations on an $FeBO_3$ single crystal were undertaken by Kamzin *et al.*[24] by comparing the Mössbauer signal detected by transmitted γ-quanta, backscattered x rays, and conversion electrons. Apart from a depth dependent gradual change of the magnetic structure in a surface region, a continuous reduction of the Néel temperature, on approaching the surface, was proposed. In the work of Kovalenko *et al.*,[25] relaxation effects were found in a near-surface layer. The crude depth information in the above experiments ($\approx$100 nm) did not allow an unambiguous characterization of the magnetic behavior of the near-surface region.

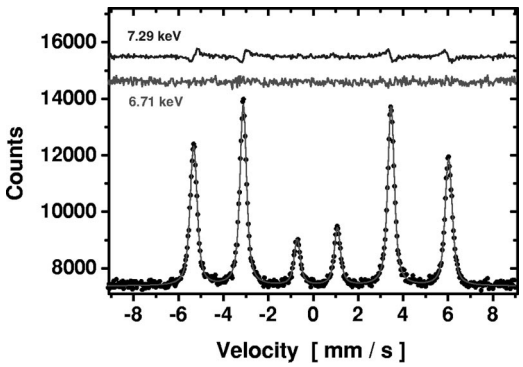

FIG. 1. Mössbauer spectrum of $FeBO_3$ at 291 K including the deviation between the measurements at 6.71 and 7.29 keV.

III. THE DCEMS METHOD

The DCEMS method is based on the coincident spectroscopy of electrons and gamma radiation.[26–28] The spectroscopy of γ radiation with high resolution is provided by the nuclear resonance absorption effect, which is called Mössbauer spectroscopy. Mössbauer spectroscopy yields the chemical and magnetic phase characterization via the hyperfine interaction of the nucleus with the electronic shell. This kind of high-resolution γ spectroscopy can be converted into a depth selective mode when detecting the subsequent conversion and Auger electrons. Their energy loss is linked to their depth of origin, i.e., the location where the Mössbauer absorption process has occurred. The random walk of the electrons by elastic and inelastic scattering can be simulated and quantified by a Monte Carlo technique. The experimental data can be deconvoluted according to these results to get the depth profile of the Mössbauer absorption.

In the DCEMS experiment both, nuclear resonance absorption and electron spectroscopy are closely linked by the convolution of the Mössbauer excitation with the electron-transport process. Due to this correlation in DCEMS, the chemical or magnetic phase resolution increases even without a precise evaluation of the depth information if one compares it to a standard Mössbauer experiment.

In its modern form, DCEMS uses an optimized setup, which, due to its highly sensitive design, makes it suitable for standard materials science characterizations.[29]

IV. EXPERIMENTAL EVIDENCE OF NEAR-SURFACE MAGNETISM IN $FeBO_3$

To get an idea of the principal hyperfine interaction in $FeBO_3$ the Mössbauer spectrum at 291 K, i.e., well below the magnetic transition point, is shown in Fig. 1. The six line pattern is reminiscent of the antiferromagnetic ordering in the sample. The intensity ratios of the individual lines mirror

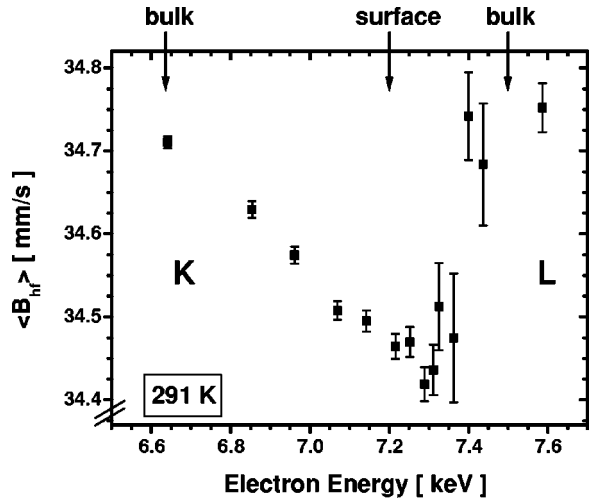

FIG. 2. Average magnetic hyperfine field at 291 K as a function of electron energy.

the perfect in-plane alignment of the atomic magnetic moments at the iron sites. The peculiar asymmetries in the spectral areas of pairs of lines, i.e., the first and sixth, second and fifth, and third and fourth lines, are due to the perpendicular orientation of the electric-field gradient and the magnetic moments. This is also seen in the relative line positions of the sextet. To demonstrate the sensitivity of the DCEMS method to minor changes in the line shape of the Mössbauer spectrum as a function of depth, the spectra for the two extreme electron energies of 6.71 (bulk like) and 7.29 keV (surface enhanced) are compared. The hyperfine parameters in the least-squares fit procedure were optimized with reference to the bulk spectrum. The spectrum at 7.29 keV that shows a surface enhancement was fitted with these parameters and the difference between experiment and theory is plotted as a horizontal line. The adequacy of the theoretical approach is seen in the flat line for the 6.71 keV case. The same characteristic deviations of the line shape show up in all resonance lines with a clear accentuation on the outmost ones. This deviation can easily be understood in terms of an appropriate magnetic hyperfine field distribution that varies towards the surface layers of the crystal. Figure 2 shows the average magnetic hyperfine field, i.e., the zero moment of the distribution, as a function of electron energy. Below 7.3 keV the *K* conversion electrons dominate in intensity, while above only *L* conversion electrons contribute to the resonant signal. K as well as *L* conversion electrons with high-energy loss transport the Mössbauer information from deeply buried layers to the electron detection system. They represent the bulk behavior of the material. However, at the *K* conversion edge at around 7.3 keV, a strong surface enhancement of the depth weight function reveals the changes in magnetic hyperfine field towards the surface. Notice the minute scale of the differences of about 1% of change.

This magnetic peculiarity of the surface is connected to the phase transition at 348.35 K. As the transition point still lies 57 K (or 0.16 in reduced units) above the room temperature measurements, the impact of the surface on the critical behavior is still weak. This will obviously change when the

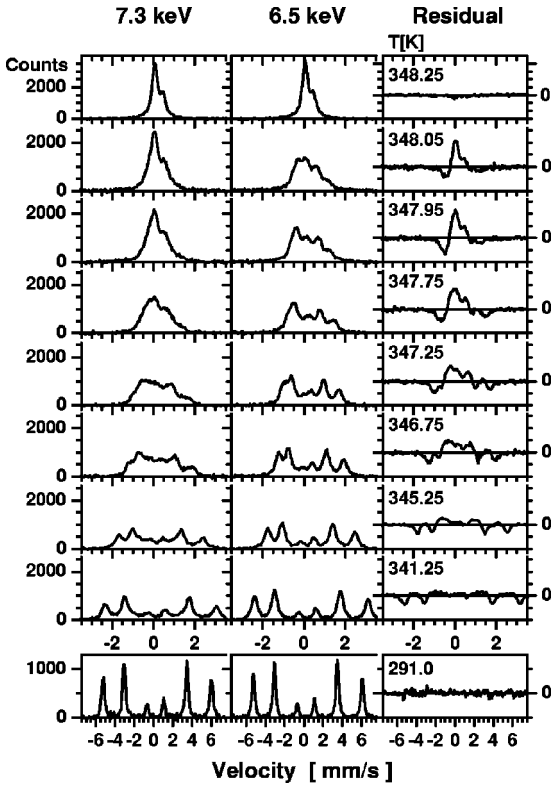

FIG. 3. Mössbauer spectra at selected temperatures for the two extreme electron energies when considering their depth weight function.

temperature is raised in a logarithmic sense towards the Néel point. Figure 3 demonstrates the systematic collapse of the magnetic hyperfine field in the 6.5 keV Mössbauer spectrum as well as the evolution of differences to the spectra measured at 7.3 keV. This is plotted in the same way as in Fig. 1 with the residual on the right. A close look at the spectra in the first two columns reveals another important feature. The bulk-like spectra are characterized by a mere shrinkage of the magnetic splitting, i.e., the relative distances between the resonance lines (the line width stays constant thus diminishing the resolution) with increasing temperature, whereas the shape of the surface sensitive spectra follows another route. A significant line broadening is followed by a strong growth of a paramagnetic fraction in the central part of the spectrum above 347.25 K. Both features hint towards a change in dynamical properties of the local magnetic moments compared to the bulk case. A final important observation is the fact that the Mössbauer spectra at these two energies approach identical shapes at very low temperatures as well as above the Néel transition. This confirms the crystallographic homogeneity of the examined sample. The paramagnetic doublet with the pronounced and ideal intensity asymmetry of the two resonance lines emphasizes the perfect orientation of the crystallographic *c* axis along the normal to the surface of the sample. The isomer shift as well as electric quadrupole splitting (QS) are plotted as a function of electron energy in Fig. 4. The depth weight functions have to be taken in the same way as in Fig. 5. Considering the extremely expanded scale of the two graphs in comparison to the natural linewidth of

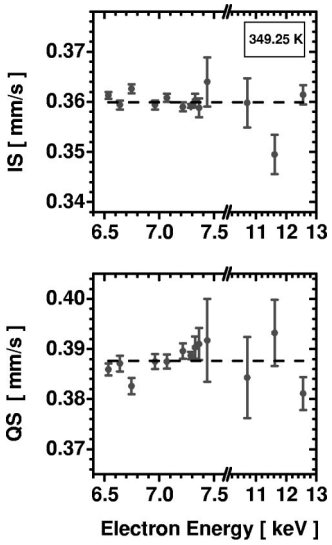

FIG. 4. Isomer shift and electric quadrupole splitting in the paramagnetic state as a function of electron energy.

the Mössbauer transition in ^{57}Fe of ≈ 0.2 mm/s, and the usual sensitivity of the line position to changes in the charge state or the crystal structure, this data again proves the high quality of the analyzed crystal. The small systematic increase of QS towards 7.4 keV could be a signature of the dangling bonds of the surface and a lattice contraction involving the first Fe monolayer.

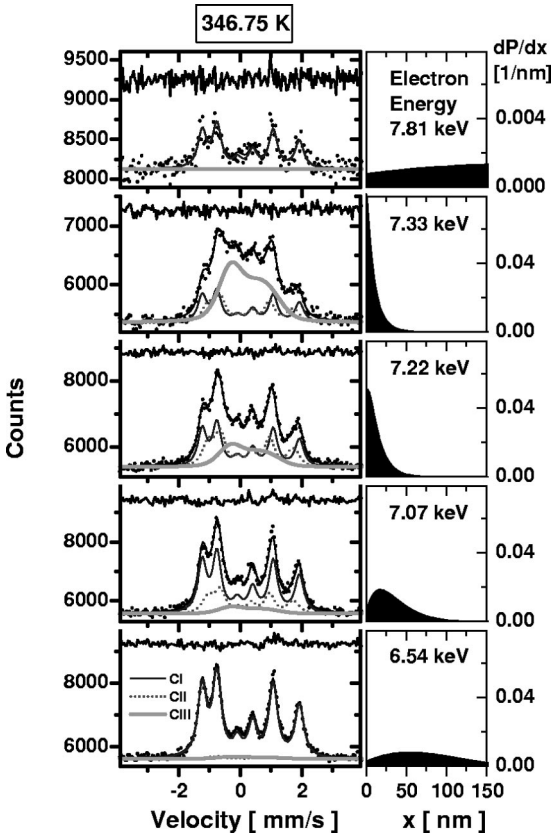

FIG. 5. A selection of Mössbauer spectra at 346.75 K at different electron energies.

V. DEPTH DEPENDENCE OF THE MAGNETIC ORDERING IN THE NEAR-SURFACE REGION

To further clarify the nature of the magnetic ordering in the near-surface region of the $FeBO_3$ single crystal, Mössbauer spectra at 346.75 K (this is 1.6 K below the Néel point) were carried out as a function of electron energy (Fig. 5). At the deepest accessible regions of the sample, i.e., at an electron energy of 6.54 keV, the Mössbauer spectrum fits perfectly in shape and splitting to what is expected for a bulk sample at this temperature (component CI). The filled graph on the right-hand side shows the appropriate depth weight function for that electron energy. Going to the other extreme of high surface sensitivity, i.e., at 7.33 keV, it is clearly visible that the spectrum is dominated by a component (CIII) that lacks the clear pattern of six lines. Nevertheless, a fraction of the spectrum still demonstrates the characteristics of the deeper regions of the sample. Both CI and CIII contributions are well separated with respect to their average hyperfine fields. Note that one does not observe a smooth transition from one extreme case to the other as the electron energy is varied. Instead, all the Mössbauer spectra between 6.54 and 7.33 keV can be deconvoluted into a mere superposition of these two extreme situations. A precise analysis of the Mössbauer data reveals an additional detail that turns out to be important for the final interpretation of the depth dependence of the hyperfine interaction. Besides the two components CI and CIII, a third contribution CII is seen with parameters that are very similar to CI but with a slightly reduced magnetic hyperfine splitting. As will be seen later, component CIII has further to be separated into two contributions as the Néel temperature is approached within 0.6 K. These will be labeled CIIIa and CIIIb.

To resolve the nature of the three components that have been determined in the Mössbauer spectra one has to take a glance at their electron spectra in Fig. 6. They are plotted as a function of temperature. The ordinate is given in absolute units of the spectral area for a relative energy resolution of 2% of the orange type spectrometer with a sample diameter of 3 mm. This allows for a comparison of the detection efficiency of different DCEMS setups. At low temperatures, component CI obviously dominates the whole Mössbauer spectrum at any electron energy. Nevertheless, due to the excellent statistical quality of the data and the entirely different nature of their respective magnetic hyperfine field distributions (as will be discussed below), components CII and CIIIa can be resolved as well.

Increasing the temperature up to 346.75 K, the following observations can be made:

(1) Component CIIIa steadily increases in intensity while CII stays constant.

(2) The electron spectrum of CIIIa does not change its shape or position.

(3) The edge of the electron spectrum of CI is flattened out and shifted to lower energies with increasing intensity of CIIIa.

(4) The position of the electron spectrum of component CII is always found in between those of CI and CIIIa, best seen in the position of its maximum.

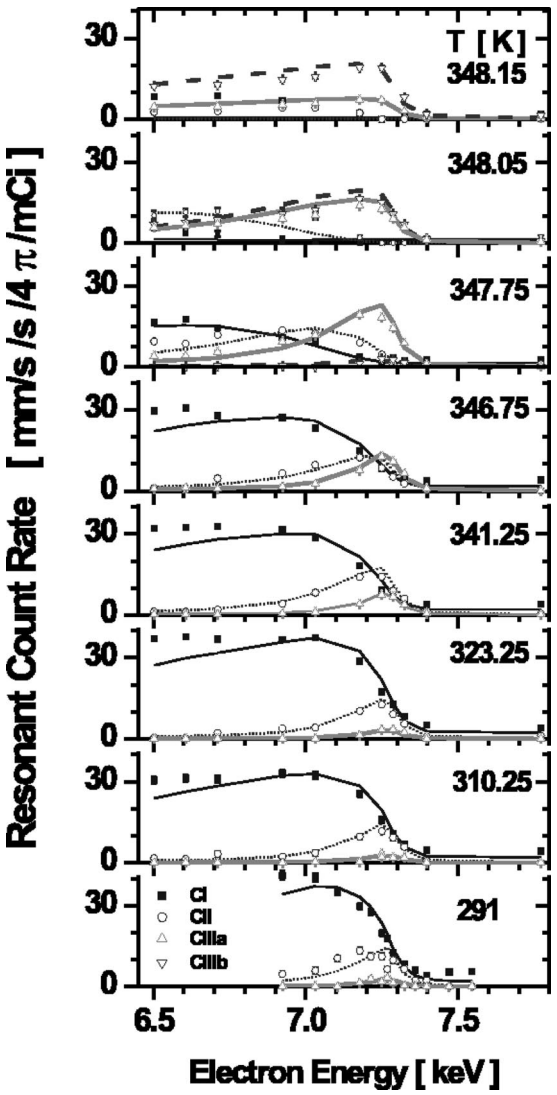

FIG. 6. Resonant electron spectra at selected temperatures. Solid lines: simulation with the discussed model. (The stronger decrease of the simulated bulk spectrum with energy loss compared to that observed in the experiment is due to transport properties that can be only seen in single-crystal spectra. They are considered to arise from electron channeling. This temperature independent effect gives a systematic uncertainty of 15% for the deconvoluted depth scale. The characteristic exponent for the temperature dependence of the surface layer thickness will not be affected.)

The points (1) to (4) summarize a general trend that is even more pronounced above 346.75 K. At 347.75 K, it becomes most apparent that the relative positions of the three resonant electron spectra obey rule (4). However, in addition to the increase in intensity, the electron spectrum of CIIIa also grows in width. Nevertheless, its edge stays at around 7.3 keV, indicating its continued presence at the very surface of the sample. In contrast to this behavior, the position of the electron spectrum of CII (though roughly maintaining its intensity, shape, and width) is shifted significantly to higher-energy losses. This represents a shift to deeper regions of the sample. In the same way, CI is driven out of this volume, retreating itself to the center of the crystal, which is not accessible to the experiment.

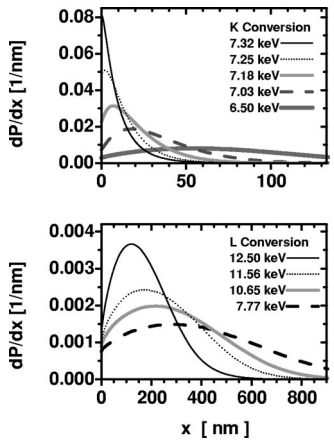

FIG. 7. Electron transport functions for $FeBO_3$ as generated from Fe transport functions by scaling according to the mass density.

Coming back to the paramagnetic fraction mentioned in the context of Fig. 3, its electron spectrum increases in intensity from 347.75 K upwards. It is labeled as CIIIb. The corresponding naming of components CIIIa and CIIIb finds its origin in the same shape of their respective electron spectra. This means, without a detailed analysis of the depth profile by a full deconvolution procedure, there is an identical depth range of both contributions. Thus, they are two signatures of the same magnetic phase.

The preceding discussion of the resonant electron spectra can be only considered as a crude description of the detailed depth profile that underlies the data. Each set of 10 to 13 Mössbauer spectra (as a function of electron energy) for each temperature point (which were about 9 in number) was analyzed simultaneously and the depth profile deconvoluted according to the depth weight functions as sketched in Fig. 7. The result of this analysis was rather surprising. Though we were expecting a gradual and smooth decrease of the magnetic order parameter (the average magnetic hyperfine field value) on approaching the surface of the sample, the only scenario that fits the Mössbauer data consistently is a completely different one. The sample consists of two depth regions that contain two different magnetic phases with entirely different properties. They are separated by some kind of a phase boundary seen as component CII in the Mössbauer spectra. With increasing temperature this phase boundary is shifted to larger depth while both phases CI and CIII persist. Such a scenario is expected for a bulk phase transition of first order, like the surface melting of water-ice.[9,30] Surprisingly, it is observed for the second-order transition of an antiferromagnet. To clarify this finding, a quantification of the evolution of the depth profile as a function of temperature has to be established. In addition, the line shapes of the Mössbauer components have to be discussed.

Looking at the temperature evolution of the separated Mössbauer fractions CI and CIII in Fig. 8, their entirely different characteristics become obvious. Let us first concentrate on the spectral shape of CI. Up to a temperature of 348 K, that is just 0.35 K below the Néel point, the typical six line pattern of (antiferro)magnetic ordering can be figured

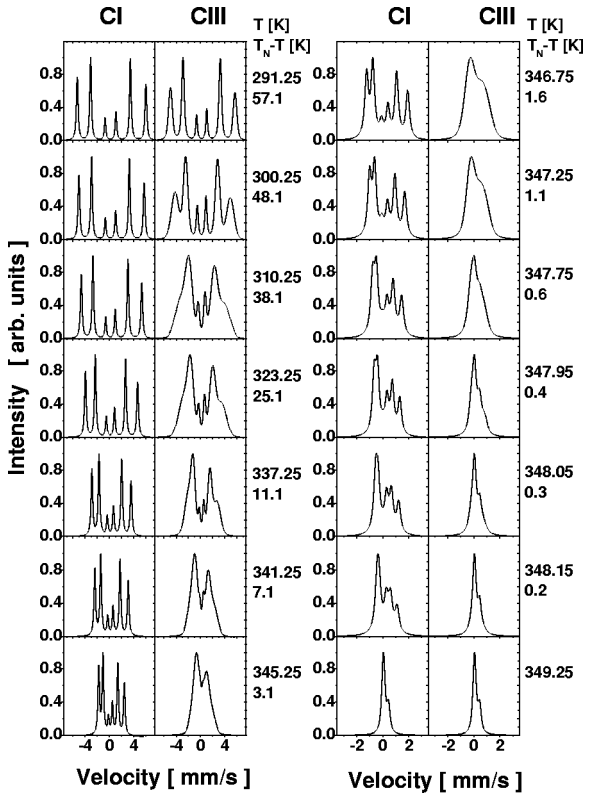

FIG. 8. Mössbauer components CI and CIII as a function of temperature.

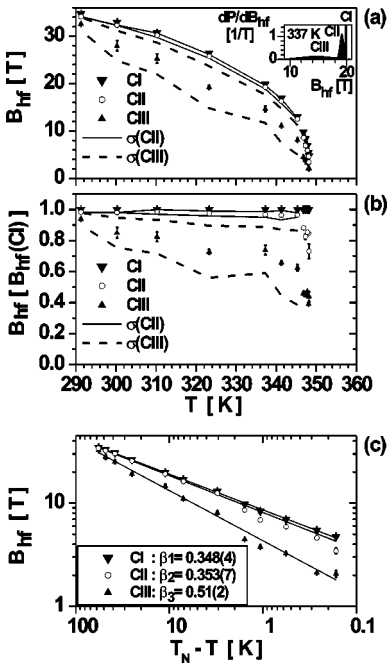

FIG. 9. Magnetic hyperfine field as a function of temperature. (a) linear plot, (b) B_{hf} normalized to the bulk hyperfine field, and (c) double logarithmic plot of B_{hf} versus $T_{Néel}$-T. Solid lines: fit to Eq. (1).

out. During the collapse of the average hyperfine field the width of the resonance lines stays constant. The plot of the well-defined magnetic hyperfine field as a function of temperature (Fig. 9) yields the typical magnetization curve of the ferromagnetic sublattice of an $FeBO_3$ single crystal. Thus, CI is representative of the bulk behavior.[31] The line shape and temperature dependence of CII is very similar to that of CI with the exception of a slightly reduced hyperfine field that exhibits a narrow distribution [see the inset in Fig. 9(a) at 337 K].

In Fig. 9(b) the magnetic hyperfine fields are plotted in units of the splitting of component CI. The hyperfine field of CII stays in a narrow range within a constant distance from CI up to temperatures of 346 K. The magnetic hyperfine field shows only a narrow distribution (solid lines). These correlated properties are due to the exchange coupling of Fe atoms in the phase boundary region CII and the adjacent layer belonging to region CI. In contrast, CIII seems to be strongly decoupled from the underlying bulk system and shows an enhanced collapse of the average magnetic hyperfine field as a function of temperature accompanied by a wide distribution. The double-logarithmic plot of Fig. 9(c) reveals the characteristic exponents that are taken according to the expression

$$B_{\mathrm{hf}}(T) = B_{\mathrm{hf}}(0)\left(1 - \frac{T}{T_{\mathrm{Néel}}}\right)^{\beta}. \qquad (1)$$

The exponents β are identical for CI and CII within the statistical error bars. The small deviations above 346 K may be due to the statistical correlation of CII with CIII. The exponent $\beta_1 = 0.348(4)$ is in agreement with Ref. 31. The more pronounced decrease with temperature for CIII is described by $\beta_3 = 0.51(2)$, following the same analytical relationship.

In summary, the expected simple behavior of the bulk component is not found in the magnetic near-surface phase. Its characteristics resemble the features of a superparamagnetic system. Up to about 1 K below the Néel transition point, the line shape, especially the line broadening of the outer pair of lines, hints to a relaxation of collective magnetic moments. The intensity ratio of the resonance lines indicates that the moments of these dynamically formed magnetic clusters fluctuate within the plane perpendicular to the *c* axis of the crystal. Later on, we will see that a detailed model of this relaxation process will lead to a quantification of its time constant. As a function of temperature it will show the expected critical slowing down on approaching the phase-transition point. Above a certain temperature, still below $T_{Néel}$, these collective relaxations along a certain preferred direction (in-plane uniaxial anisotropy) will convert to a complete directional switching behavior. As in superparamagnetism, this will lead to the appearance of a paramagnetic fraction in the center of the Mössbauer spectra (Fig. 8).

Before going into further detail, let us have a look at the temperature-dependent depth scale of the phenomenon. This scale is easily defined by the thickness of the near-surface region that contains the newly discovered magnetic phase. This quantity is plotted along with the thickness of the phase boundary between CI and CIII in Fig. 10, in an appropriate double-logarithmic plot. In a phase transition of second order one expects the thickness $D(T)$ of the region that is modified

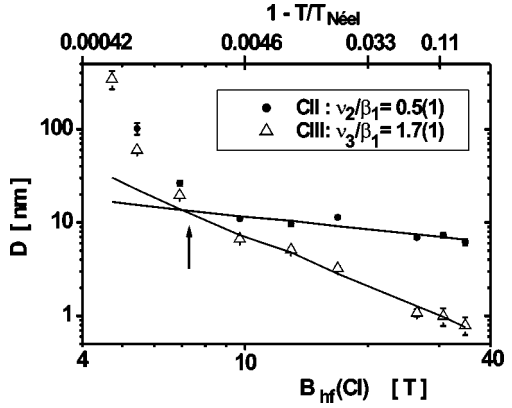

FIG. 10. Evolution of the depth profile as a function of reduced temperature (triangles: thickness of near-surface phase, circles: thickness of phase boundary). Solid lines according to Eq. (2). The arrow indicates the appearance of the paramagnetic fraction CIIIb close to the Néel temperature.

by the influence of the surface to scale with the same power law as the correlation length ξ:

$$D(B_{\mathrm{hf}}) = D_0 B_{\mathrm{hf}}^{-\nu/\beta_1} \sim \left(1 - \frac{T}{T_{\mathrm{Néel}}}\right)^{-\nu} \sim \xi(T). \qquad (2)$$

From Fig. 10 it is clear that for $B_{hf} \geqslant 10$ T, i.e., $T_{\mathrm{Néel}} - T \geqslant 2$ K, the thickness DII and DIII follow this behavior. The multiplication of the exponent for DIII $\nu_3/\beta_1 = 1.7(1)$ by β_1 leads to the characteristic exponent $\nu_3 = 0.59(4)$, which is identical to the theoretical value 0.63 of the magnetic correlation length of the bulk system. The temperature dependence of DII is much weaker and gives $\nu_2/\beta_1 = 0.5(1)$. This fits into the picture of a phase boundary region with a more or less constant thickness.

Above 346.5 K, the divergence of the thicknesses DII and DIII are much stronger than the extrapolated power law. This coincides with an onset of a strong line broadening of component CII and the appearance of the paramagnetic fraction of component CIII. The paramagnetic fraction indicates the switching of the local magnetic moments between opposite directions of the easy axis. The switching occurs on a time scale that is shorter than 10^{-8} s.

VI. DYNAMICS

Concentrating now on the dynamical aspects of the critical system the evaluation of the Mössbauer line shape can reveal a crude idea of the relaxation time in the near-surface phase CIII. According to Wegener[32] the collective relaxations of magnetic moments should lead to a characteristic line broadening. The line broadening (given in mm/s) does not scale in a simple linear fashion with the average magnetic hyperfine field. Rather, a scaling proportional to the average squared fluctuation of the hyperfine field $\langle \Delta B_{\mathrm{hf}}^2 \rangle$ is predicted as

$$\Gamma = \Gamma_0 + \frac{2c(0.243\mu_n \langle B_{\mathrm{hf}} \rangle)^2}{14.4 \text{ keV } \hbar} \tau \langle \Delta B_{\mathrm{hf}}^2 \rangle. \qquad (3)$$

Γ_0 represents the experimental linewidth without the relaxation effects, c the velocity of light, $\mu_n = 31.5 \times 10^{-9}$ eV/T the nuclear magneton, and τ the relaxation time of the atomic moment. $2\pi\hbar/0.243\mu_n\langle B_{\mathrm{hf}}\rangle$ constitutes the nuclear Larmor precession time where $\langle B_{\mathrm{hf}} \rangle$ is the average value of the hyperfine field while the average squared fluctuation of B_{hf} is given by

$$\langle \Delta B_{\mathrm{hf}}^2 \rangle = \langle (B_{\mathrm{hf}} - \langle B_{\mathrm{hf}} \rangle)^2 \rangle = \langle B_{\mathrm{hf}}^2 \rangle - \langle B_{\mathrm{hf}} \rangle^2. \qquad (4)$$

To determine τ, i.e., the time scale of the collective dynamics of the atomic moments, an estimate of the quadratic fluctuation $\langle \Delta\ B_{\mathrm{hf}}^2 \rangle$ has to be obtained. The average hyperfine field has to be taken from the near-surface phase ($\langle B_{\mathrm{hf}}^{\text{near-surface}} \rangle$), which is a function of temperature (Fig. 9). The physical reason for this choice is the necessity to distinguish between the rather short-time scale (compared to the nuclear Larmor frequency) of the fluctuations of the individual atomic moments due to spin-lattice relaxation and the longer-time scale of the collective fluctuations of a cluster of atomic moments relative to the magnetic easy axis. The latter crosses the nuclear Larmor precession time at a certain temperature, thus leading to the experimentally observed line broadening. As this effect scales linearly with $\langle B_{\mathrm{hf}}^{\text{near-surface}} \rangle$ it is clear that the collapse of the average hyperfine field near $T_{\mathrm{Néel}}$ will limit the experimental observation above a certain temperature. On the other hand, at lower temperatures, the collective fluctuations will be frozen out and only the relaxation free experimental line width will be measured. In other words, there is only a small temperature interval where the relaxation effects can be evaluated quantitatively. As we will see later, the results, nevertheless, cover a time interval of four orders in magnitude.

To get an idea of $\langle \Delta B_{\mathrm{hf}}^2 \rangle$ as a function of temperature, one has to bring to mind the following picture: similar to the situation in small particles, the collective relaxation of clusters of magnetic moments [their average size is temperature dependent through the correlation length ξ(T)] will take place along the direction of the magnetic easy axis. However, in contrast to the small particle case and in accordance with the above experimental observations (Mössbauer line intensities), the fluctuation is confined to a plane. The simplest approach[33] for the potential of the collective moment is given by

$$E(\theta) = KV \sin^2 \theta, \qquad (5)$$

where K is the magnetocrystalline anisotropy, V, the volume of the cluster, and θ, the angle between the easy axis and the collective moment. The temperature-dependent probability density for any direction specified by the polar angle θ can then be expressed as

$$P(\theta) \sim e^{-(KV/kT)\sin^2\theta}. \qquad (6)$$

In the three dimensional case an additional factor of $\sin\theta$ would appear in the expression for $P(\theta)$. Choosing the abbreviations $a = kT/KV$, $x = \sin\theta$, and $\sqrt{1-x^2} = \cos\theta$, the projected hyperfine field as well as its quadratic deviation

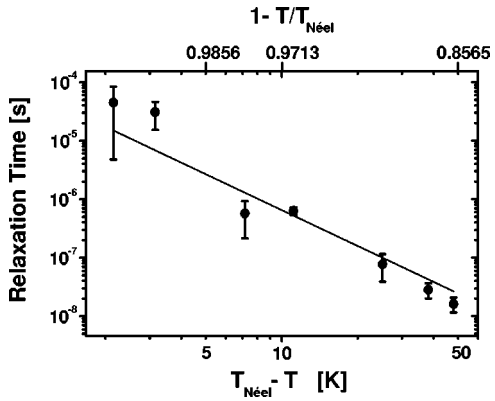

FIG. 11. Relaxation time of the magnetic clusters showing the critical slowing down near the Néel temperature.

can be determined analytically with the help of the given probability function. The following integrals will be used for this purpose:

$$\int_0^1 P(x)\frac{dx}{\sqrt{1-x^2}}=\frac{\pi}{2}e^{-1/2a}I_0\left(\frac{1}{2a}\right), \tag{7}$$

$$\langle\cos\theta\rangle=\int_0^1 P(x)dx=\frac{1}{2}\sqrt{a}\sqrt{\pi}\,\mathrm{Erf}\left(\frac{1}{\sqrt{a}}\right), \tag{8}$$

$$\langle\cos\theta^2\rangle=\int_0^1 P(x)\sqrt{1-x^2}dx=\frac{\pi}{4}e^{-1/2a}\left[I_0\left(\frac{1}{2a}\right)+I_1\left(\frac{1}{2a}\right)\right]. \tag{9}$$

$I_n(x)$ defines the modified Bessel function of the first kind of order n. Erf(x) is the error function. Equation (7) gives the normalization of the probability. The expression in Eq. (9) is the first step to evaluate Eq. (3) as it is proportional to the projected quadratic fluctuation of the collective moment which generates the hyperfine field. The average value of the hyperfine field will be proportional to $\langle\cos\theta\rangle$ as given in Eq. (8).

The next step is to elucidate the physical meaning of K and V, especially with respect to their temperature variation. In terms of the reduced temperature $t=1-T/T_{\mathrm{Néel}}$ and the critical exponents $\beta=0.348(4)$, $\nu=0.63$, and νz (from $\tau\sim t^{-\nu z}$, the temperature dependence of the correlation time) the following expressions can be written down:

$$K(t)=K_0t^{3\beta}\approx K_0t \tag{10}$$

gives the temperature-dependence of the uniaxial magnetocrystalline anisotropy. As has been mentioned, the temperature-dependent average volume of the magnetic clusters should be given by the magnetic correlation length:

$$V(t)=b\xi^3\sim t^{-3\nu}\approx t^{-2}. \tag{11}$$

Hence, the product KV will approximately follow the power law 1/t. More generally $1/a$ will obey

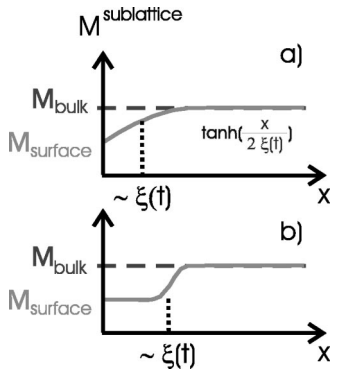

FIG. 12. Depth profile of the order parameter: (a) expected and (b) measured.

$$\frac{1}{a}=\frac{KV}{kT}=\frac{K_0bt^{3(\beta-\nu)}}{kT}=\left(1-\frac{T}{T_{\mathrm{Néel}}}\right)^{3(\beta-\nu)}\frac{K_0b}{kT}. \tag{12}$$

This expression for a can be introduced into the Eqs. (7) to (9). Together with Eq. (3) and the temperature dependence of the mean magnetic hyperfine field, the theory can be fitted to the experimental line broadening data with $I_0=K_0b$ and z as free parameters.

Figure 11 shows the development of the relaxation time τ as a function of reduced temperature t. It reveals the expected slowing down towards the Néel temperature, which is an increase of the correlation time in the self-correlation function of the atomic moment. The exponent of the power law is $\nu z=2.0$ ($\pm$ 0.9) which fits into the theoretically expected range.[34] As a reverse conclusion, the assumption in Eq. (11) with respect to the relationship between the volume $V(t)$ and the correlation length $\xi(t)$, seems to hold good.

VII. DISCUSSION

The DCEMS results demonstrate that in the near-surface region of an $FeBO_3$ single crystal an unexpected magnetic phase is formed on an approach to the Néel transition from below. This phase is separated from the bulk region of the crystal by a phase boundary that could be detected in the Mössbauer experiments. The thickness of the magnetically distinct near-surface region follows a power law as a function of reduced temperature with a critical exponent of $\nu_3=0.59(4)$. This value is identical to the theoretical value of the corresponding exponent of the correlation length $\xi^{\mathrm{bulk}}(t)$ in the three-dimensional Ising bulk system.[35–38] The depth profile of the near-surface phase is expected to scale with $\xi^{\mathrm{bulk}}(t)$.[9,39]

Regarding Fig. 3 (7.3 keV) and Fig. 8 (component CIII) magnetic correlations are still seen in the near-surface region up to the Néel point. Though the respective Mössbauer spectra close to $T_{\mathrm{Néel}}$ look very much like those of the pure paramagnetic state, the measured line width has still not reached the low value of the paramagnet. In other words, the phase transition at the surface occurs at the same temperature as the bulk system with an uncertainty of 0.1 K. Thus, we are dealing with the so-called ordinary case of a surface-phase transition.

Putting together this last point and the temperature dependence of the length scale of the near-surface region one would expect a depth profile of the magnetic order parameter $M(x,t)$ according to Fig. 12(a),[9] namely,

$$M(x,t)=\tanh\left(\frac{x}{2\ \xi(t)}\right). \tag{13}$$

What is observed experimentally for the mean of the order parameter is a depth dependence as shown in Fig. 12(b), which would be in agreement with a bulk phase transition of first order. That is not the case as can be seen from the magnetization curves in Fig. 9. The determined depth profile of the order parameter according to Fig. 12(b) is usually connected with the surface melting in solid-liquid phase transitions. This surface wetting is well known for water-ice[9,30,40,41] in the temperature interval of $-13\,^{\circ}\mathrm{C}$ to $0\,^{\circ}\mathrm{C}$. It was studied with glancing incidence x-ray diffraction. Surface wetting is not confined to the melting of water-ice alone, but has also been observed on a lead surface with a proton channeling technique.[42] A similar behavior can be found in order-disorder transitions at antiphase boundaries when studied with a transmission electron microscope[43–47] or at free surfaces measured with x-ray scattering.[48,49]

Coming back to the magnetic system, the order parameter exhibits (in addition to the wetting phenomenon) a distribution function that originates from the relaxation dynamics of the spin system at any temperature. From the Mössbauer line shape in the appropriate temperature interval, it can be deduced that collective moments are formed in accordance with the magnetic correlation length. Thus the average size of the magnetic clusters correlates to the thickness of the near-surface phase. The collective moments show a characteristic relaxation along the in-plane easy axis of the system. The related relaxation time could be measured over four orders of magnitude. Looking at the temperature dependence of the order parameter it has to be pointed out that the critical exponent $\beta_3=0.51(2)$ lies between the bulk value and the surface value of $\beta=0.8$ for the semi-infinite Heisenberg model.[34,50,51] The value of 0.51 coincides with the value found by Watson *et al.*[13,52] for the surface of UO_2.

The origin of the observed discrepancies with the theoretical predictions are not yet clear. To elucidate the situation, a second single crystal of $FeBO_3$ doped with Ga was analyzed with the DCEMS technique. 24% of the Fe had been replaced by Ga (checked by Rutherford backscattering spectroscopy). This would weaken the magnetic interaction between the Fe moments. Temperature as well as depth dependent measurements were carried out. In Fig. 13 the Mössbauer spectra of the bulk signal are plotted as a function of temperature. At 67 K the spectrum is composed of a sextet with symmetrical resonance lines. As the temperature increases an asymmetrical line broadening is observed. This reflects that the magnetic interaction of the Fe atoms here are more complicated as compared to the pure $FeBO_3$ crystal. The present state of data analysis does not allow a distinction between pure structural effects (Ga distribution) and dynamical aspects. The Néel temperature is reduced to around 265 K, as expected for the weakened exchange interaction of the Fe moments.

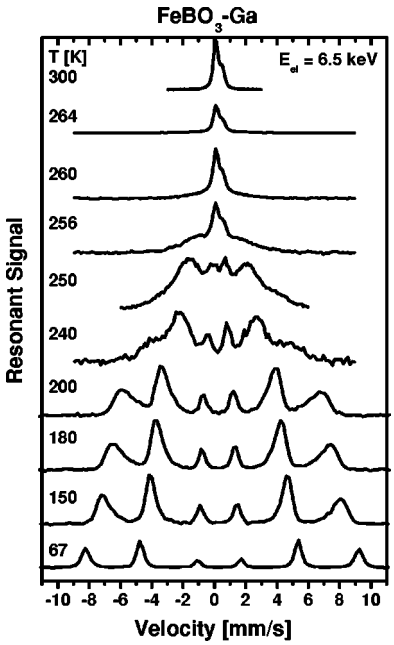

FIG. 13. Temperature-dependent Mössbauer spectra for the Ga doped crystal.

The plotted Mössbauer spectra have to be compared to those spectra that have increased surface sensitivity. For the sake of simplicity, a subset of only five spectra has been selected for that purpose. In Fig. 14 the phase transition can be followed between 67 and 300 K. Looking at the shape of the spectra for both electron energies, no significant differences are observed. This means that the underlying hyperfine interaction is of the same nature. Nevertheless, the temperature scale of the two data sets is different. Note especially that the intermediate temperature values differ by roughly 10 K. This means that the surface transition exhibits a lower order parameter value at the intermediate temperatures compared to the bulk transition. However, in contrast to the pure $FeBO_3$ crystal, the shape of the spectra in the two sets are

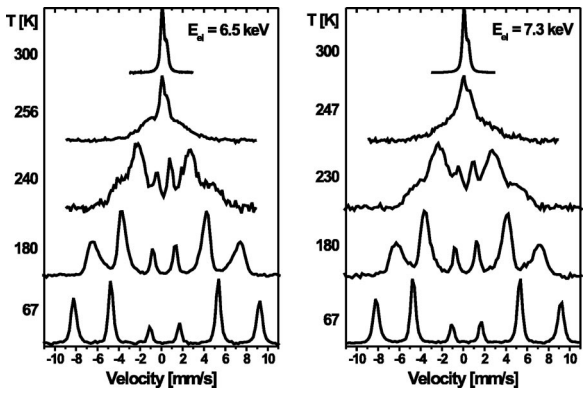

FIG. 14. Subset of temperature-dependent Mössbauer spectra for the $(Fe_{0.76}Ga_{0.24})BO_3$ crystal at the two electron energies 6.5 and 7.3 keV.

similar. This is exactly what is expected if the order-parameter profile follows a behavior as plotted in Fig. 12(a).

According to the present state of analysis, the substitution of about 1/4 of the Fe by Ga changes the magnetic interaction in a way that the near-surface region of the crystal obeys perfectly the theoretical predictions of an ordinary surface phase transition in the presence of a bulk transition of second order. Considering the fact that the Fe-O-Fe superexchange interaction is blocked by Ga atoms, it becomes obvious why the critical behavior near the surface of the pure $FeBO_3$ crystal is not observed in the case of the $(Fe_{0.76}Ga_{0.24})BO_3$ sample. An essential feature of the near-surface phase in the pure crystal is the dynamical formation of magnetic clusters that behave similarly to small magnetic particles. The average size of these clusters as well as the thickness of the near-surface region is determined by the magnetic correlation length $\xi^{\mathrm{bulk}}(t)$. Only in the pure crystal $\xi^{\mathrm{bulk}}(t)$ can develop its characteristic temperature dependence that holds homogeneously for the whole crystal. In the Ga doped crystal the local fluctuations in the Ga concentration will break the homogeneity of the magnetic system. This will lead to a local variation of the correlation length $\xi^{\mathrm{bulk}}(t,\vec{x})$. The primary consequence of this will be that a magnetically distinct but homogenous (in the time average) layer of constant thickness D(t) cannot be formed any longer on top of the bulk system. Under this condition, and on the background of the spatially varying strength of the superexchange interaction, the dynamical formation of magnetic clusters will be weakened. They will be subjected to stronger statistical variations. In other words, the unexpected magnetic features of the pure $FeBO_3$ crystal have their origin in the well defined but temperature-dependent magnetic correlations between neighboring Fe atoms.

As in a phase transition of first order, the magnetic-phase separation between the bulk and the near-surface region of the pure $FeBO_3$ crystal is preferred energetically to the expected gradual decrease of the order parameter with depth, in accordance with Eq. (13). This implies that the magnetic near-surface phase with its dynamic properties entails a reduction of energy of the entire system. This over compensates for the cost in energy of maintaining the phase boundary that separates the surface and bulk regions.

*Author to whom correspondence should be addressed. Also at Institut für Nanotechnologie, Forschungszentrum Karlsruhe, 76021 Karlsruhe, Germany. Email address: branko.stahl@hrzpub.tu-darmstadt.de

[1] L. Néel, J. Phys. Radium **15**, 225 (1954); M.I. Kaganov, Sov. Phys. JETP **61**, 1679 (1971); D.L. Mills, Phys. Rev. B **3**, 3887 (1971); T. Kaneyoshi, J. Phys. C **3**, 4497 (1991); A.J. Freeman and Ru-qian Wu, J. Magn. Magn. Mater. **100**, 497 (1991).

[2] A. N. Bogdanov and U. K. Rossler, Phys. Rev. Lett. **87**, 037203 (2001).

[3] A. N. Bogdanov, U.K. Rossler, and K. H. Müller, J. Magn. Magn. Mater. **238**, 155 (2002).

[4] M. E. Fisher, *Critical Phenomena*, edited by M. S. Green (Academic, London 1971).

[5] K. Binder and P. C. Hohenberg, Phys. Rev. B **6**, 3461 (1972).

[6] K. Binder and P. C. Hohenberg, Phys. Rev. B **9**, 2194 (1974).

[7] H. W. Diehl, *Phase Transitions and Critical Phenomena*, edited by C. Domb and J. L. Lebowitz (Academic Press, London 1983), Vol. 10.

[8] H. Wagner, *Applications of Field Theory to Statistical Mechanics*, Lecture Notes in Physics Vol. 216, edited by L. Garrido (Springer-Verlag, Heidelberg 1985).

[9] H. Dosch, *Critical Phenomena at Surfaces and Interfaces: Evanescent X-Ray and Neutron Scattering*, Springer Tracts in Mod. Phys. Vol. 126 (Springer-Verlag, New York, 1992).

[10] A. H. Morrish and K. Haneda, J. Magn. Magn. Mater. **35**, 105 (1983).

[11] T. Shinjo, Surf. Sci. Rep. **12**, 49 (1991); *Studies of Magnetic Properties of Fine Particles and their Relevance to Materials Science*, edited by J. L. Dormann and D. Fiorani (Elsevier Science, B. V., 1992).

[12] U. Gradmann, Appl. Phys. Lett. **3**, 161 (1974); J. Magn. Magn. Mater. **100**, 481 (1991); S. Duncan, A. H. Owens, R. J. Semper, J. C. Walker, Hyperfine Interact. **4**, 886 (1978); G. Bayreuther and G. Lugert, J. Magn. Magn. Mater. **35**, 50 (1983).

[13] G. M. Watson, D. Gibbs, G. H. Lander, B. D. Gaulin, L. E. Berman, Hj. Matzke, and W. Ellis, Phys. Rev. Lett. **77**, 751 (1996).

[14] B. Stahl, E. Kankeleit, R. Gellert, M. Müller, and A. Kamzin, Phys. Rev. Lett. **84**, 5632 (2000).

[15] E. Gerdau and R. Rüffer, H. Winkler, W. Tolksdorf, C. P. Klages, and J. P. Hannon, Phys. Rev. Lett. **54**, 835 (1985).

[16] E. Gerdau and H. de Waard, Hyperfine Interact. **123/124**, 835 (1999).

[17] A.M. van der Kraan, Phys. Status Solidi A **18**, 215 (1973).

[18] T. Shinjo, M. Kiyama, N. Sugita, K. Watanabe, and T. Takada, J. Magn. Magn. Mater. **35**, 133 (1983).

[19] T. Yang, A. Krishnan, N. Benczer-Koller, and G. Bayreuther, Phys. Rev. Lett. **48**, 1292 (1982).

[20] B. Stahl, R. Gellert, M. Müller, E. Kankeleit, and A. Kamzin, Hyperfine Interact. **126**, 371 (2000).

[21] B. Stahl, M. Ghafari, H. Hahn, A. Kamzin, and D. Hanzel, Mater. Res. Soc. Symp. Proc. **676**, Y7.6.1 (2001).

[22] G.N. Belozersky, *Mössbauer Studies of Surface Layers* (Elsevier, New York, 1993); K. Nomura, Y. Ujihira, and A. Vertes, J. Radioanal. Nucl. Chem. **202**, 103 (1996).

[23] D. Liljequist, J. Phys. D **16**, 1567 (1983); **11**, 839 (1978).

[24] A. Kamzin and L. A. Grigor'ev, Sov. Phys. Solid State **36**, 694 (1994).

[25] P. P. Kovalenko, V. G. Labushkin, A. K. Ovsepyan, E. R. Sarkisov, E. V. Smirnov, and I. G. Tolpekin, Sov. Phys. Solid State **29**, 340 (1987).

[26] E. Kankeleit, Z. Phys. **164**, 442 (1961).

[27] E. Moll and E. Kankeleit, Nukleonik **7**, 180 (1965).

[28] T. Bonchev, A. Jordanov, and A. Minkova, Nucl. Instrum. Methods **70**, 36 (1969).

[29] B. Stahl and E. Kankeleit, Nucl. Instrum. Methods Phys. Res. B **122**, 149 (1997).

[30] J. G. Dash, Haiying Fu, J. S. Wettlaufer, Rep. Prog. Phys. **58**, 115 (1995).

[31] M. Eibschütz, L. Pfeiffer, and J. W. Nielsen, J. Appl. Phys. **41**, 1276 (1970).

[32] H. Wegener, Z. Phys. **186**, 498 (1965).

[33] F. Bodker, M. F. Hansen, C. B. Koch, K. Lefmann, and S. Mørup, Phys. Rev. B **61**, 6826 (2000).
[34] H. W. Diehl and S. Dietrich, Z. Phys. B: Condens. Matter **42**, 65 (1981); **43**, 315 (1981).
[35] G. S. Pawley, R. H. Swendsen, D. J. Wallace, and K. G. Wilson, Phys. Rev. B **29**, 4030 (1984).
[36] J. C. Le Guillou and J. Zinn-Justin, *Phase Transitions*, edited by M. Levy, J.C. Le Guillou, and J. Zinn-Justin (Plenum, New York, 1982).
[37] C. J. Hamer, J. Phys. A **16**, 1257 (1983).
[38] J. Adler, J. Phys. A **16**, 3585 (1983).
[39] K. Binder, *Phase Transitions and Critical Phenomena* Vol. 8, edited by C. Domb and J. L. Lebowitz (Academic, New York, 1983).
[40] A. Lied, H. Dosch, and J. H. Bilgram, Phys. Rev. Lett. **72**, 3554 (1994).
[41] H. Dosch, Appl. Phys. A: Solids Surf. **61**, 475 (1995).
[42] W. Joost, M. Frenken, and J. F. van der Veen, Phys. Rev. Lett. **54**, 134 (1985).
[43] P. R. Swann, W. R. Duff, R. M. Fisher, Phys. Status Solidi **37**, 577 (1970).
[44] A. Finel, V. Mazauric, and F. Ducastelle, Phys. Rev. Lett. **65**, 1016 (1990).
[45] Ch. Ricolleau, A. Loiseau, F. Ducastelle, R. Caudron, Phys. Rev. Lett. **68**, 3591 (1992).
[46] D. Le Floc'h, A. Loiseau, Ch. Ricolleau, C. Barreteau, R. Caudron, F. Ducastelle, J. M. Penisson, Phys. Rev. Lett. **81**, 2272 (1998).
[47] Y. Le Bouar, A. Loiseau, A. Finel, and F. Ducastelle, Phys. Rev. B **61**, 3317 (2000).
[48] S. F. Alvarado, M. Campagna, A. Fattah, and W. Uelhoff, Z. Phys. B: Condens. Matter **66**, 103 (1987).
[49] H. Dosch, L. Mailänder, A. Lied, J. Peisl, F. Grey, R. L. Johnson, and S. Krummacher, Phys. Rev. Lett. **60**, 2382 (1988).
[50] K. Ohno, Y. Okabe, and A. Morita, Prog. Theor. Phys. **71**, 714 (1984).
[51] K. Binder and D.P. Landau, Phys. Rev. Lett. **52**, 318 (1984).
[52] G. M. Watson, D. Gibbs, G. H. Lander, B. D. Gaulin, L. E. Berman, Hj. Matzke, and W. Ellis, Phys. Rev. B **61**, 8966 (2000).